Editors' Suggestion

# Signatures of a Nonthermal Metastable State in Copropagating Quantum Hall Edge Channels

Kosuke Itoh,[1] Ryo Nakazawa,[1] Tomoaki Ota,[1] Masayuki Hashisaka,[1,2] Koji Muraki,[2] and Toshimasa Fujisawa[1,*]
[1]*Department of Physics, Tokyo Institute of Technology, 2-12-1 Ookayama, Meguro, Tokyo 152-8551, Japan*
[2]*NTT Basic Research Laboratories, NTT Corporation, 3-1 Morinosato-Wakamiya, Atsugi 243-0198, Japan*

(Received 22 November 2017; published 11 May 2018)

A Tomonaga-Luttinger (TL) liquid is known as an integrable system, in which a nonequilibrium many-body state survives without relaxing to a thermalized state. This intriguing characteristic is tested experimentally in copropagating quantum Hall edge channels at bulk filling factor $\nu = 2$. The unidirectional transport allows us to investigate the time evolution by measuring the spatial evolution of the electronic states. The initial state is prepared with a biased quantum point contact, and its spatial evolution is measured with a quantum-dot energy spectrometer. We find strong evidence for a nonthermal metastable state in agreement with the TL theory before the system relaxes to thermal equilibrium with coupling to the environment.

DOI: 10.1103/PhysRevLett.120.197701

Electron-electron interaction in usual conductors is often considered to bring the system into a thermalized state irrespective of the initial states [1–3]. In the case of one-dimensional Tomonaga-Luttinger (TL) liquids with interacting electrons, the integrable TL model suggests the presence of many conserved quantities and the absence of thermalization processes [4–6]. In the presence of weak nonintegrable interactions, the system exhibits two-stage equilibration from an initial nonequilibrium state through an intermediate nonthermal metastable state to a thermalized state [7,8]. While such intriguing dynamics have been observed in ultracold atoms [9,10], solid-state realization would open vast nonequilibrium many-body physics particularly for transporting massive information. Edge channels in the integer quantum Hall regime can host a chiral TL liquid, particularly at bulk Landau level filling factor $\nu = 2$ with spin-up and -down edge channels [11,12]. Electrons in the channels are mutually interacting, and collective excitation (plasmon) modes appear as the charge and spin (or dipole) modes, which have symmetric and antisymmetric charge distribution, respectively, for the two channels if the drift velocity difference is negligible [13]. This spin-charge separation has been identified in various measurements such as time- and spin-resolved measurement [14,15], frequency-domain plasmon interference [16], and shot-noise detection [17]. A promising scheme for studying the equilibration dynamics is quantum-dot (QD) energy spectroscopy for a nonequilibrium state prepared by a biased quantum point contact (QPC) [8,18], where nonthermal states can be identified by observing non-Fermi distribution functions. Although the previous work [19] was successful in observing a spectral change, the nonthermal metastable state was not resolved, as the resulting spectrum looked like a Fermi distribution function. As this can be explained by either the TL model [20] or a stochastic scattering model [21], conclusive evidence is highly desirable.

In this Letter, we have used the same QD-QPC scheme but have investigated systematically to see how the energy distribution function changes with the initial state and the traveling distance. The expected nonthermal metastable state is successfully identified with an arctangent distribution function by setting the QPC at a low tunneling probability. The spectral change in the first equilibration is consistent with the plasmon excitations based on the TL model. The second equilibration toward cold Fermi distribution suggests weak coupling to the environment. In this way, the edge channels provide a unique opportunity for studying the integrability in a solid-state system.

Figure 1(a) shows a schematic measurement setup for investigating copropagating edge channels, $C_\uparrow$ for spin up and $C_\downarrow$ for spin down, alongside a two-dimensional electron system (2DES) at $\nu = 2$ under a perpendicular magnetic field $B$. The two Ohmic contacts on both ends are always grounded at base temperature $T_{\mathrm{base}}$. Nonequilibrium charge is injected from similar $\nu = 2$ edge channels, shown in the lower left, with bias voltage $V_{\mathrm{S}}$ through a QPC at conductance $(e^2/h)D$. Here, channel $C_\uparrow$ can be excited by spin-up tunneling at $0 < D < 1$, and $C_\downarrow$ by spin-down tunneling at $1 < D < 2$. The charge flows to the downstream, and the electronic state at a distance $L$ from the QPC is investigated by a QD spectrometer with an energy level $\varepsilon$ that can be tuned with the QD gate voltage $V_{\mathrm{QD}}$. With appropriate bias voltage $V_{\mathrm{D}}$ on similar $\nu = 2$ edge channels in the lower right, the current $I_{\mathrm{D}}(\varepsilon)$ through the dot level can be made proportional to the energy distribution function $f_\uparrow(\varepsilon)$ in channel $C_\uparrow$ as described below.

 

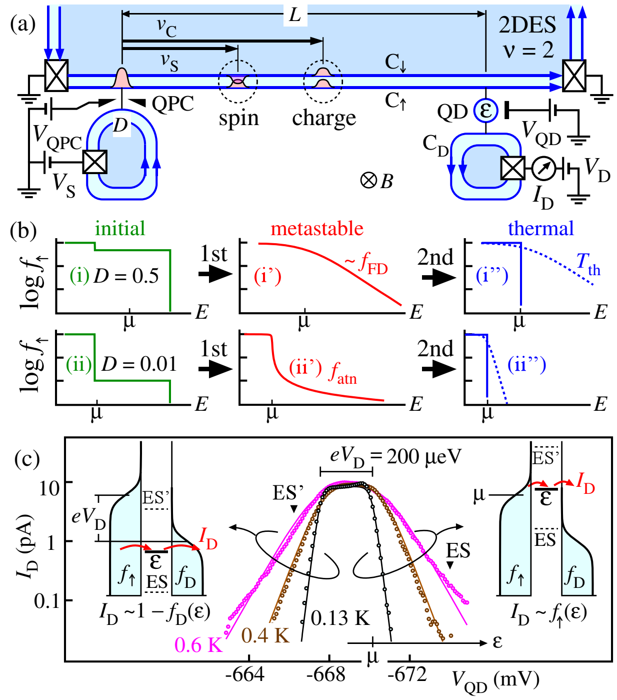


FIG. 1. (a) Schematic setup for the energy spectroscopy on copropagating channels $C_\uparrow$ and $C_\downarrow$. (b) Expected two-stage equilibration from initial states with double-step distribution function in panel (i) at $D = 0.5$ and (ii) at $D = 0.01$, through metastable states in (i′) and (ii′), to thermalized states in (i″) and (ii″) with dashed lines for a closed system and solid lines for an open system. (c) Current profiles of the QD spectrometer at various lattice temperatures. The energy diagrams in the left and right insets show that the currents on the left and right sides are proportional to the distribution functions $1 - f_D$ and $f_\uparrow$, respectively. Current through ES (ES′) is allowed only when the ground state at $\varepsilon$ is occupied (empty).

The initial energy distribution function in $C_\uparrow$ is expected to be a double-step function with height $D$ and width $eV_S$ by assuming energy-independent tunneling probability, as shown in panel (i) for $D = 0.5$ and (ii) for $D = 0.01$ in Fig. 1(b). For $D < 1$, one may consider that single electrons are randomly injected to $C_\uparrow$ at a rate of $(e/h)DV_S$. The uncertainty relation implies that each electron wave packet has a spread $h/eV_S$ in time, and $vh/eV_S$ in space, for velocity $v$ in the channel. The coupling between $C_\uparrow$ and $C_\downarrow$ splits each wave packet into charge and spin wave packets, as illustrated in Fig. 1(a) [15]. The length required for the spin-charge separation is given by $\ell_{SC} = hv_{SC}/eV_S$ with the relative velocity $v_{SC} = v_C v_S/(v_C - v_S)$ for charge and spin velocities $v_C$ and $v_S$, respectively. Levkivskyi and Sukhorukov have calculated the energy distribution function at large distances beyond the spin-charge separation length $\ell_{SC}$ [8]. It is close to, but should be slightly different from, the Fermi distribution function $f_{FD}(E) = [1 + e^{(E-\mu)/k_B T_{th}}]^{-1}$ at thermalization temperature $T_{th} = \sqrt{\frac{3}{2}}(1/\pi k_B)\sqrt{D(1-D)}eV_S$ when the tunneling is frequent at $D \simeq 0.5$ [panel (i′) in Fig. 1(b) for $D = 0.5$]. Here, $\mu$ is the corresponding chemical potential. In contrast, when the tunneling events are sparse ($D \ll 1$), a nonthermal metastable state with a nontrivial distribution function of an arctangent form $f_{atn}(E) = \frac{1}{2} - \arctan(E/\Gamma)/\pi$ (a Lorentzian function in $df/dE$ [8]) is expected to emerge with $\Gamma = 2eDV_S/\pi$ [panel (ii′) for $D = 0.01$]. Intriguingly, no scattering happens even when a fast charge wave packet overtakes a slow spin wave packet, and thus there should be no further thermalization processes in the integrable model. Actual devices may have other thermalization processes. If the thermalization is associated with the nonintegrable interaction within the channel, the system may relax to a heat-conserved thermalized state with a Fermi distribution function at $T_{th}$ [the dashed lines in panels (i″) and (ii″)] after a long travel. If the system is weakly coupled to the environment, the system relaxes to a thermalized state at $T_{base}$ (the solid lines). We shall investigate such two-stage equilibration.

We used a couple of devices with different lengths $L$ ranging from 0.12 to 15 $\mu$m between the QD and QPC [22]. They are fabricated in standard AlGaAs/GaAs heterostructures with electron densities of 2.9 and $3.1 \times 10^{11}$ cm$^{-2}$ and low-temperature mobilities of 1.6 and $1.9 \times 10^6$ cm$^2$/V s, and measured at $B = 6$ and 7.5 T, respectively, for $L \geq 5$ and $L \leq 0.5$ $\mu$m devices in a dilution refrigerator at $T_{base} = 80$–110 mK. Finite current in $I_D$ is observed when the energy level $\varepsilon$ of the ground state is located in the transport window of the width $eV_D$ (typically 200 $\mu$eV), as shown in Fig. 1(c). The temperature dependence shows a clear heating effect in both sides of the peak. All traces are fitted nicely with the Fermi distribution function over more than 2 orders of magnitude. As shown in the insets, $I_D$ is proportional to $f_\uparrow$ on the right side, where we focus in the following measurements, and to $(1 - f_D)$ with the distribution function $f_D$ in the drain channel $C_D$ on the left side. In practice, excited states in the QD may contribute additional current [22]. The downward triangles labeled ES and ES′ in all plots represent the conditions of excited states being aligned to one of the chemical potentials in the channels. Data in Fig. 1(c) show that the excited states play a minor role when the channels show Fermi distribution functions.

Now, we investigate nonequilibrium states with the QPC. First, we focus on the first equilibration occurring at $L \sim \ell_{SC}$. Since $\ell_{SC}$ is tunable with $V_S$, the first equilibration can be studied with varying $L$ and $\ell_{SC}$. Here, $\ell_{SC}$ is estimated by using $v_{SC} = 27$ km/s, obtained in the following analysis. As summarized in Figs. 2(a) and 2(b), the double-step current profile is clearly resolved in trace (i) taken at $L = 0.12\,\mu\mathrm{m} \ll \ell_{SC} = 1.1\,\mu\mathrm{m}$ ($V_S = 100$ $\mu$V), but gradually smeared out, as seen in traces (ii) at $L = 0.5$ $\mu$m $< \ell_{SC} = 1.1$ $\mu$m and (iii) at $L = 0.5$ $\mu$m $\sim \ell_{SC} = 0.7$ $\mu$m ($V_S = 150$ $\mu$V). Their step positions were

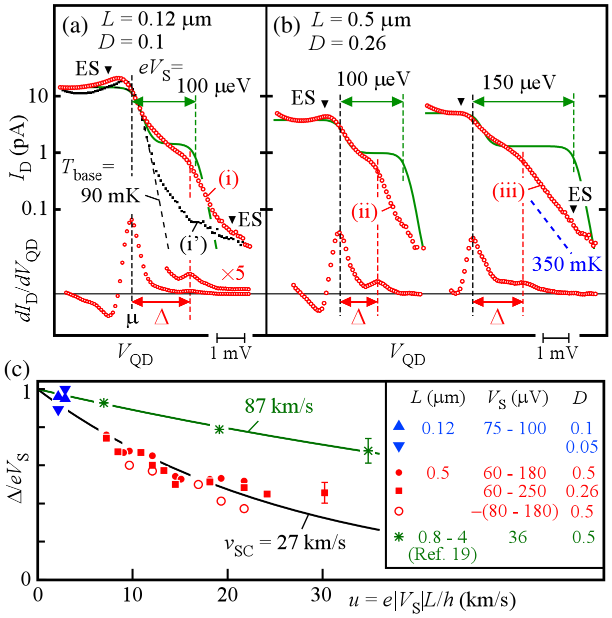


FIG. 2. (a) and (b) QD current profiles and their derivatives on the right side of the current peak. The double-step feature is clear in (i), but it is smeared out with reduced step distance $\Delta$ in (ii) at longer $L$, and in (iii) at larger $V_S$. The reference trace (i′) for the background excitation level is taken under opposite chirality. The black dashed curve in (a) shows $f_{FD}$ at $T_{base} = 90$ mK. The green solid lines show the initial double-step function at $T_{base}$. (c) The normalized step distance $\Delta/eV_S$ as a function of $u \equiv e|V_S|L/h$. The solid lines are exponential fits to our data with $v_{SC} = 27$ km/s and the data in Ref. [19] with 87 km/s.

determined from the peak positions in the derivative (lower traces). The distance between the two steps, $\Delta$ evaluated in energy, deviates from the original step width $eV_S$ with increasing $L$ and $V_S$.

Figure 2(c) summarizes the normalized step width $\Delta/eV_S$ as a function of the interaction strength defined by $u \equiv e|V_S|L/h$. Data points taken at various $L$, $V_S$, and $D$ values follow single monotonic functions (solid lines). As we are not aware of a theoretical formula for this dependence, an exponential dependence $\Delta/eV_S = \exp(-L/\ell_{SC}) = \exp(-u/v_{SC})$ is assumed for the solid lines, with $v_{SC} = 27$ km/s for our devices and 87 km/s for the devices in Ref. [19] with an additional surface gate. These values are close to $v_{SC} = 60$–$75$ km/s, obtained from a time-of-flight experiment in Ref. [15]. The variation may stem from the different geometries of the metal gate that partially screens the interaction [26–28]. Note that the observed $V_S$ dependence in Fig. 2(c) does not agree with the *stochastic* electron-electron scattering approach [29], where the energy loss $(eV_S - \Delta)$ is found to be independent of $V_S$. Our systematic study supports that the first-stage equilibration is associated with the *deterministic* spin-charge separation.

Let us investigate the energy distribution function at $L > \ell_{SC}$. Figure 3(a) shows the current profile taken at $L = 5\ \mu$m and $D = 0.005$, where unusual distribution functions with a long tail appear. We find excellent agreement with the theoretically predicted arctangent function (the red solid lines), where the single parameter $\Gamma = 2hI_S/\pi e$ was determined from the measurement of $I_S$. As $\ell_{SC}$ decreases with increasing $V_S$, no significant departure from the arctangent function is seen even at the longest relative distance $L/\ell_{SC}$, reaching 28 at $V_S = 600\ \mu$V ($\ell_{SC} = 0.18\ \mu$m).

To identify the region where the nonthermal state emerges, the QD current spectra in Fig. 3(c) are taken at various $D$ values ranging from 0 to 2 marked by red circles in the QPC conductance steps of Fig. 3(b). While nearly Fermi distribution [showing a straight line in the low-current region of Fig. 3(c)] appears under frequent tunneling conditions $D \simeq 0.5$ and $D \simeq 1.5$, non-Fermi distribution with a tail (marked by red regions) is observed under sparse tunneling conditions $0 < D < 0.3$, $0.7 < D < 1.3$, and $1.7 < D < 2$. Quantitatively similar behavior is observed for the spin-up ($0 < D < 1$) and spin-down ($1 < D < 2$) tunneling, consistent with the interpretation that the energy

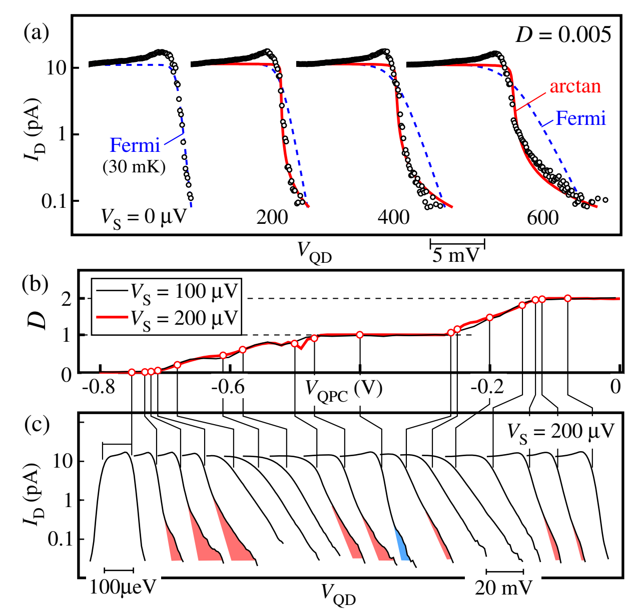


FIG. 3. (a) $V_S$ dependence of the QD current profile obtained at small $D = 0.005$, showing an excellent agreement with the arctangent function (the red solid lines). No features approaching the Fermi distribution function (the blue dashed lines for $T_{th}$) are seen. A peak near the Fermi edge is associated with the Fermi edge singularity [22]. (b) Gate voltage $V_{QPC}$ dependence of the dimensionless conductance $D$ of the QPC, where the series resistance in the setup is subtracted. (c) QD current profiles at various $D$ values marked by open circles in (b). The nonthermal current tail in (c) is highlighted by red and blue regions. The small tail in the blue region for $D = 1$ might be induced by spin-flip tunneling between the channels. Each profile in (a) and (c) is offset horizontally for clarity. The width of the current peak at $D = 0$ in (c) corresponds to $eV_D = 100\ \mu$eV.

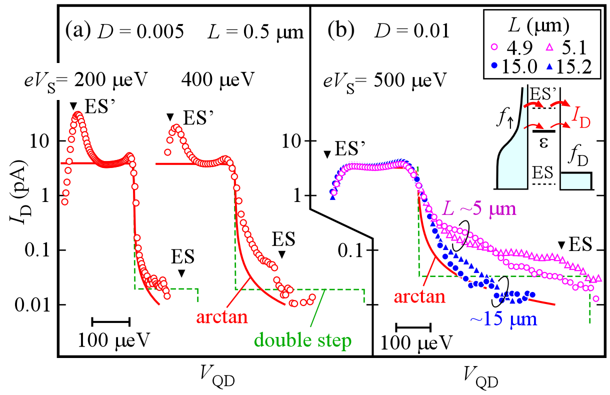


FIG. 4. (a) QD current profiles at $L \simeq 0.5$ $\mu$m. (b) QD current profiles at $L \simeq 5$ and 15 $\mu$m. The unusual current tail is observed in all traces. The tail is larger than expected (the solid line for the arctangent function) due to the excess current through ES′ as shown in the inset. The dashed lines show the double-step function at $T_{\rm base} = 0$. The inset shows the energy diagram for QD spectroscopy with excited states, ES and ES′.

exchange occurs via spin-charge separation. Detailed analysis on this data is shown in the Supplemental Material [22].

If the current tail is associated with the nonthermal state of the TL model, it should be stable for long traveling before the second equilibration comes in. As shown in Fig. 4(a), nonthermal states showing nonexponential current tails are well developed at $L = 0.5$ $\mu$m close to $\ell_{\rm SC} = 0.55$ $\mu$m ($V_{\rm S} = 200$ $\mu$V) and greater than $\ell_{\rm SC} = 0.28$ $\mu$m ($V_{\rm S} = 400$ $\mu$V). Similar current profiles are also seen at much longer distances, $L \simeq 5$ and 15 $\mu$m as compared to $\ell_{\rm SC} = 0.22$ $\mu$m ($V_{\rm S} = 500$ $\mu$V) in Fig. 4(b). Although they were measured in slightly different conditions with different samples, quite similar current profiles showing a long tail are reproduced in the wide range of $L$. This manifests the long-lived nature of the nonthermal state.

The data in Fig. 4(b) were measured using the same QD spectrometer, while the excitation was done with different QPCs. Although the QPC characteristics are slightly different, the long tail of the distribution function seems to be attenuated as $L$ increases from 5 to 15 $\mu$m. Similar attenuation with the decay length of about $\ell_{\rm leak} = 20$ $\mu$m is also seen at $D = 0.5$ and $V_{\rm S} = 200$ $\mu$V [22]. This suggests heat leakage to the environment. Although we need further studies to identify its origin, it could be related to spin-flip tunneling between the channels [30,31], plasmon scattering with counterpropagating channels [26,32,33], excitation in remote channels [34], and coupling to phonons [35,36].

In this way, the expected nonthermal metastable state is clearly demonstrated. The evidence is reinforced by the following arguments excluding experimental artifacts.

We performed similar experiments at the reversed magnetic field where, due to opposite chirality, plasmon excitations cannot reach the QD detector. We observed no measurable influence on $I_{\rm D}$ at $L \geq 0.5$ $\mu$m. A small excess current for the shortest distance of $L = 0.12$ $\mu$m [trace (i′) at $B = -7.5$ T in Fig. 2(a)] is possibly due to photon assisted tunneling via electrostatic coupling between the QPC and the QD [37]. This ensures that the current tail observed at $B > 0$ is associated with the chiral plasmons in the edge channel.

Spin-flip tunneling between $C_\uparrow$ and $C_\downarrow$ can influence the distribution function. This effect should be maximized at $D = 1$, where we observed in a separate measurement with the same sample that about 0.5% of injected electrons in $C_\uparrow$ experience tunneling to $C_\downarrow$ during the propagation of 15 $\mu$m at $V_{\rm S} = 200$ $\mu$V [30,31]. This unwanted excitation might be the reason for having a small current tail (the blue region) at $D = 1$ in Fig. 3(c). The spin-flip tunneling should play a minor role at $D \ll 1$.

The QPCs used in this work show nonlinear current-voltage characteristics [22,38]. The QPC used for Fig. 3 shows reasonable linearity up to 200 $\mu$V, where the data in Fig. 3(c) were taken, as shown by the small difference between the QPC conductance steps at $V_{\rm S} = 100$ and 200 $\mu$V in Fig. 3(b). The linearity holds even up to $V_{\rm S} \simeq 500$ $\mu$V for small $D = 0.005$, where the clear arctangent profile in Fig. 3(a) is obtained. Therefore, the nonlinearity should play a minor role in the appearance of nonthermal states. However, the nonlinearity can deflect or increase the distribution function from the expected arctangent form, which could be the case for the data of Fig. 4 [22].

While the calculated current profiles presented here were obtained by solving rate equations with the ground state of the QD only, we also checked the effects of excited states [22,39]. For Fermi distribution functions, the inclusion of the excited states in the simulation did not change the current profile significantly. In contrast, for arctangent functions, the current profile changed considerably when the excited states had larger tunneling rates than the ground state. This also explains why the observed current in Fig. 4 is greater than the calculated one with the ground state only. We note that in Fig. 3 the measured current in the tail agrees well with the calculation, where this QD shows small tunneling rates for the excited states [22].

In summary, we have successfully observed nonthermal states with arctangent energy distribution functions. This suggests that the system can be regarded as an effectively closed quantum many-body system for a limited length ($< \ell_{\rm leak}$), despite the fact that Ohmic contacts and the measurement apparatus are attached. This would open the way to exploring many-body quantum dynamics in the solid states [40].

We thank Yasuhiro Tokura and Keiji Saito for fruitful discussions. This work was supported by JSPS KAKENHI (No. JP26247051 and No. JP15H05854), the International Research Center for Nanoscience and Quantum Physics at Tokyo Institute of Technology, and the Nanotechnology Platform Program of MEXT.

*fujisawa@phys.titech.ac.jp


[1] J. Gemmer, M. Michel, and G. Mahler, *Quantum Thermodynamics*, Lecture Notes in Physics Vol. 784 (Springer, Berlin Heidelberg, 2009).
[2] B. L. Altshuler and A. G. Aronov, Electron-electron interaction in disordered conductors, in *Electron-Electron Interactions in Disordered Systems*, edited by A. L. Efros and M. Pollak (North-Holland Physics Publishing, Amsterdam, 1985), p. 1.
[3] H. Pothier, S. Guéron, N. O. Birge, D. Esteve, and M. H. Devoret, Phys. Rev. Lett. **79**, 3490 (1997).
[4] T. Giamarchi, *Quantum Physics in One Dimension* (Oxford University Press, Oxford, England, 2004).
[5] D. B. Gutman, Y. Gefen, and A. D. Mirlin, Phys. Rev. Lett. **101**, 126802 (2008).
[6] A. Iucci and M. A. Cazalilla, Phys. Rev. A **80**, 063619 (2009).
[7] A. Polkovnikov, K. Sengupta, A. Silva, and M. Vengalattore, Rev. Mod. Phys. **83**, 863 (2011).
[8] I. P. Levkivskyi and E. V. Sukhorukov, Phys. Rev. B **85**, 075309 (2012).
[9] T. Kinoshita, T. Wenger, and D. S. Weiss, Nature (London) **440**, 900 (2006).
[10] M. Gring, M. Kuhnert, T. Langen, T. Kitagawa, B. Rauer, M. Schreitl, I. Mazets, D. A. Smith, E. Demler, and J. Schmiedmayer, Science **337**, 1318 (2012).
[11] Z. F. Ezawa, *Quantum Hall Effects: Field Theorectical Approach and Related Topics* (World Scientific Publishing, Singapore, 2008).
[12] A. M. Chang, Rev. Mod. Phys. **75**, 1449 (2003).
[13] E. Berg, Y. Oreg, E.-A. Kim, and F. von Oppen, Phys. Rev. Lett. **102**, 236402 (2009).
[14] V. Freulon, A. Marguerite, J. M. Berroir, B. Plaćais, A. Cavanna, Y. Jin, and G. Féve, Nat. Commun. **6**, 6854 (2015).
[15] M. Hashisaka, N. Hiyama, T. Akiho, K. Muraki, and T. Fujisawa, Nat. Phys. **13**, 559 (2017).
[16] E. Bocquillon, V. Freulon, J. M. Berroir, P. Degiovanni, B. Plaćais, A. Cavanna, Y. Jin, and G. Fève, Nat. Commun. **4**, 1839 (2013).
[17] H. Inoue, A. Grivnin, N. Ofek, I. Neder, M. Heiblum, V. Umansky, and D. Mahalu, Phys. Rev. Lett. **112**, 166801 (2014).
[18] C. Altimiras, H. le Sueur, U. Gennser, A. Cavanna, D. Mailly, and F. Pierre, Nat. Phys. **6**, 34 (2010).
[19] H. le Sueur, C. Altimiras, U. Gennser, A. Cavanna, D. Mailly, and F. Pierre, Phys. Rev. Lett. **105**, 056803 (2010).
[20] D. L. Kovrizhin and J. T. Chalker, Phys. Rev. Lett. **109**, 106403 (2012).
[21] A. M. Lunde, S. E. Nigg, and M. Büttiker, Phys. Rev. B **81**, 041311 (2010).
[22] See Supplemental Material http://link.aps.org/supplemental/10.1103/PhysRevLett.120.197701 for experimental details device characteristics, QD spectroscopy, and nonthermal spectra, which includes Refs. [23–25].
[23] K. Tobias, C. Livio, R. Christian, W. Werner, G. Leonid, I. Thomas, and E. Klaus, New J. Phys. **19**, 023009 (2017).
[24] A. S. Goremykina and E. V. Sukhorukov, Phys. Rev. B **95**, 155419 (2017).
[25] J. von Delft and H. Schoeller, Ann. Phys. (N.Y.) **7**, 225 (1998).
[26] M. G. Prokudina, S. Ludwig, V. Pellegrini, L. Sorba, G. Biasiol, and V. S. Khrapai, Phys. Rev. Lett. **112**, 216402 (2014).
[27] N. Kumada, H. Kamata, and T. Fujisawa, Phys. Rev. B **84**, 045314 (2011).
[28] $v_{\mathrm{SC}}$ is sensitive to $v_{\mathrm{S}}$ rather than $v_{\mathrm{C}}$. The effect of the metallization on $v_{\mathrm{S}}$ is not understood well.
[29] A. M. Lunde and S. E. Nigg, Phys. Rev. B **94**, 045409 (2016).
[30] S. Komiyama, H. Hirai, M. Ohsawa, Y. Matsuda, S. Sasa, and T. Fujii, Phys. Rev. B **45**, 11085 (1992).
[31] G. Müller, D. Weiss, A. V. Khaetskii, K. von Klitzing, S. Koch, H. Nickel, W. Schlapp, and R. Lösch, Phys. Rev. B **45**, 3932 (1992).
[32] K. Washio, R. Nakazawa, M. Hashisaka, K. Muraki, Y. Tokura, and T. Fujisawa, Phys. Rev. B **93**, 075304 (2016).
[33] H. Kamata, N. Kumada, M. Hashisaka, K. Muraki, and T. Fujisawa, Nat. Nanotechnol. **9**, 177 (2014).
[34] M. Hashisaka, H. Kamata, N. Kumada, K. Washio, R. Murata, K. Muraki, and T. Fujisawa, Phys. Rev. B **88**, 235409 (2013).
[35] N. Telang and S. Bandyopadhyay, Phys. Rev. B **48**, 18002 (1993).
[36] M. G. Prokudina, V. S. Khrapai, S. Ludwig, J. P. Kotthaus, H. P. Tranitz, and W. Wegscheider, Phys. Rev. B **82**, 201310 (2010).
[37] E. Onac, F. Balestro, L. H. Willems van Beveren, U. Hartmann, Yu. V. Nazarov, and L. P. Kouwenhoven, Phys. Rev. Lett. **96**, 176601 (2006).
[38] V. Venkatachalam, S. Hart, L. Pfeiffer, K. West, and A. Yacoby, Nat. Phys. **8**, 676 (2012).
[39] T. Fujisawa, D. G. Austing, Y. Tokura, Y. Hirayama, and S. Tarucha, J. Phys. Condens. Matter **15**, R1395 (2003).
[40] A. Calzona, F. M. Gambetta, F. Cavaliere, M. Carrega, and M. Sassetti, Phys. Rev. B **96**, 085423 (2017).